

AugServe: Adaptive Request Scheduling for Augmented Large Language Model Inference Serving

Ying Wang
Zhejiang University
China

Zhen Jin
Zhejiang University
China

Jiexiong Xu
Zhejiang University
China

Wenhai Lin
Alibaba Group
China

Yiquan Chen
Alibaba Group
China

Wenzhi Chen^{*}
Zhejiang University
China

Abstract

As augmented large language models (LLMs) with external tools become increasingly popular in web applications, improving augmented LLM inference serving efficiency and optimizing service-level objectives (SLOs) are critical for enhancing user experience. To achieve this, inference systems must maximize request handling within latency constraints, referred to as increasing effective throughput. However, existing systems face two major challenges: (i) reliance on first-come-first-served (FCFS) scheduling causes severe head-of-line blocking, leading to queuing delays exceeding the SLOs for many requests; and (ii) static batch token limit, which fails to adapt to fluctuating loads and hardware conditions. Both of these factors degrade effective throughput and service quality.

This paper presents *AugServe*, an efficient inference framework designed to reduce queueing latency and enhance effective throughput for augmented LLM inference services. The core idea of *AugServe* is a two-stage adaptive request scheduling strategy. Specifically, *AugServe* combines the inference features of augmented LLM requests to optimize the order of scheduling decisions (stage I). These decisions are continuously refined with runtime information (stage II), adapting to both request characteristics and system capabilities. In addition, *AugServe* dynamically adjusts the token batching mechanism based on hardware status and real-time load, further enhancing throughput performance. Experimental results show that *AugServe* achieves 4.7-33.1× and 3.3-13.2× higher effective throughput than vLLM and InferCept, while reducing time-to-first-token (TTFT) by up to 96.3% and 95.0%, respectively.

1 Introduction

Augmented Large Language Models (LLMs) have rapidly emerged as a promising paradigm in modern web services [1, 15]. In contrast to traditional text-only LLMs, which rely on fixed pretrained parameters and lack real-time knowledge [11, 29], augmented LLMs extend their capabilities by

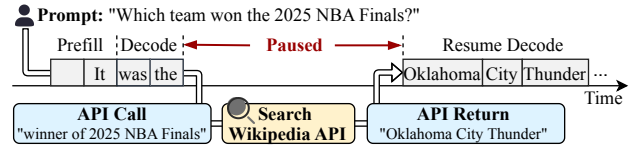


Figure 1: Augmented LLM inference process.

invoking external tools (e.g., web APIs, database, or specialized models) during inference [6, 7, 14, 22, 23, 27, 29]. This approach enables augmented LLMs to perform more complex tasks such as arithmetic computation [5, 15, 36], real-time information retrieval [11, 33], and web interactions [26, 40], gradually positioning them as a core component of web services.

Augmented LLM inference service systems are becoming the key infrastructure for next-generation web services, with their inference efficiency directly impacting user experience. Figure 1 illustrates the workflow of the augmented LLM inference service [1, 13]. (i) During inference, the augmented LLM identifies the need for real-time information and triggers the corresponding tool calls. (ii) The inference process is then paused while awaiting the response from the external augmentation module. (iii) Once the response is returned, the serving system appends it to the sequence generated and resumes normal generation. Additionally, inference systems need to efficiently handle large numbers of concurrent user requests, which must meet **service-level objective (SLO)** requirements [3, 12, 25, 35, 42] (e.g., requiring time-to-first-token (TTFT) below a fixed threshold [12]). Therefore, inference systems must maximize request handling within latency constraints [3, 20, 38]. This metric, commonly referred to as **effective throughput** or **goodput**, is defined as the number of completed requests meeting SLOs per unit time, reflecting a system’s real-time performance.

State-of-the-art research focuses on improving inference performance. vLLM [21] introduces PageAttention to optimize GPU memory utilization. However, in augmented LLM inference, vLLM treats external calls as request termination and discards the request’s context (i.e., Key-Value (KV) cache). When the call returns, costly recomputation is

^{*} Corresponding author

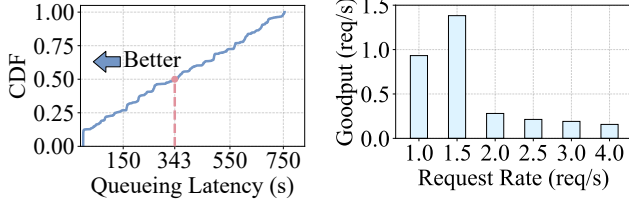


Figure 2: Queueing latency (s) distribution of InferCept under 4.0 req/s request rate.

required, causing severe GPU memory and computational resource waste. InferCept [1] proposes dynamic context handling during external calls, selecting among discarding the KV cache, preserving it in GPU memory, or swapping it to CPU, based on call duration and context length. This approach reduces resource waste and improves augmented LLM inference efficiency.

However, existing inference systems still face two challenges in improving the effective throughput of augmented LLM inference:

C1: Excessive queueing delays that break SLOs . In existing service systems, many requests experience queueing times far beyond SLOs requirements, sharply degrading goodput. Frameworks such as vLLM and InferCept typically rely on first-come-first-served (FCFS) scheduling, where long requests block short ones, causing severe head-of-line (HoL) blocking and higher latency. In augmented LLM inference, long context handling policies during external calls and uncertainty in return length further amplify the HoL problem and increase queueing delays. Figure 2 and 3 illustrate the queueing latency distribution and effective throughput of InferCept with OPT-13B on an H800 GPU, using a merged augmented LLM workload [1]. As shown in Figure 2, 50% of requests at 4.0 req/s have queueing delays exceeding 343s, far surpassing SLOs (e.g., TTFT < 1s). Moreover, Figure 3 shows that when the load exceeds 2.0 req/s, the number of completed requests per second meeting SLOs drops considerably. This strict arrival-order scheduling severely limits effective throughput under high-load augmented LLM inference.

C2: Static batch token limit restricts throughput improvement. In augmented LLM inference, the lengths of inputs, outputs, and API responses vary significantly across requests. A fixed batch token limit fails to adapt to dynamic workloads, where overly small limit leads to fewer requests being processed per iteration and lower throughput, whereas an excessively large limit causes resource contention and redundant recomputation.

In this paper, we propose *AugServe*, an efficient inference serving framework designed to reduce request queueing latency and improve effective throughput for augmented LLM inference services. We introduce a **two-stage adaptive request scheduling strategy (C1)**, which adaptively makes scheduling decisions based on the features of augmented LLM infer-

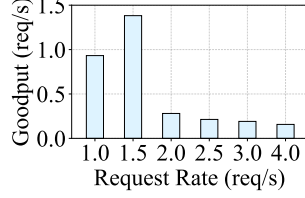


Figure 3: Effective throughput (req/s) of InferCept under different request rates.

ence requests and runtime information, effectively addressing HoL blocking and reducing queueing delays. Additionally, we propose a **dynamic token-level batching mechanism (C2)**, which dynamically sets the batch token limit based on real-time load and system conditions. By combining these two mechanisms, *AugServe* effectively adapts to request demands and load fluctuations, significantly improving the service performance of the augmented LLM inference.

For the two-stage scheduling, we focus on the external call features of augmented LLM inference requests, including call duration, return length, and context handling policies. By combining these with request input and output length, we design a decision-making approach to evaluate each request’s scheduling value in terms of waiting time and memory usage. A small model is employed to predict call duration and output length for guiding scheduling value computation. Using the value, the most suitable requests are selected for batching in each iteration to minimize overall queueing delay (Stage I). Furthermore, to better adapt to system status, we dynamically refine the scheduling value based on actual external call return lengths and context handling policies (Stage II). Otherwise, an anti-starvation mechanism is introduced to ensure fairness.

For dynamic token-level batching, we propose dynamically setting the batch token limit based on the external call patterns, real-time load, and hardware memory usage, maximize throughput while meeting SLOs under varying workloads. Furthermore, we impose bounded constraints to prevent extreme cases, thereby ensuring system stability while improving inference efficiency.

We implemented *AugServe* on vLLM and evaluated its performance against both vLLM and InferCept using two LLMs, GPT-J-6B [34] and OPT-13B [39], across various hardware platforms (NVIDIA RTX 4090, H800, and A100 GPUs). Overall, *AugServe* demonstrates superior latency and effective throughput performance compared to both baseline systems. *AugServe* achieves 4.7-33.1× and 3.3-13.2× higher effective throughput than vLLM and InferCept, while reducing TTFT by up to 96.3% and 95.0%, respectively.

In summary, our contributions are as follows:

- We introduce *AugServe*, an efficient inference serving framework for augmented LLMs, which reduces request queueing latency and improves effective throughput. (§4)
- We design a two-stage adaptive request scheduling strategy that adaptively optimizes request scheduling order based on request features and runtime information. (§4.3)
- We develop a dynamic token-level batching mechanism that adjusts the batch token limit adapting to real-time load. (§4.4)
- We conduct extensive evaluations to confirm that *AugServe* outperforms vLLM and InferCept in inference performance (§5).

2 Background

2.1 Augmented Large Language Models

As LLMs rapidly evolve, their text-only capabilities and fixed model parameters have exposed limitations, such as hallucinations and lack of real-time knowledge [8, 11, 29], making them inadequate for growing application demands. To address these issues, augmented LLMs integrate external tools and resources (e.g., web APIs, database queries, external models) during inference [6, 7, 14, 22, 23, 27, 29], enhancing their ability to perform diverse tasks like arithmetic computation [5, 15, 36] and real-time web interaction [26, 40].

Meanwhile, with the popularization of Function Calling [24] and the Model Context Protocol (MCP) [4], invoking external tools has also become increasingly prevalent within LLM inference services [1, 9, 13, 23], enabling support for more diverse user needs. Consequently, augmented LLM inference systems are gradually emerging as the core infrastructure for modern web applications.

2.2 Existing LLM Inference Systems

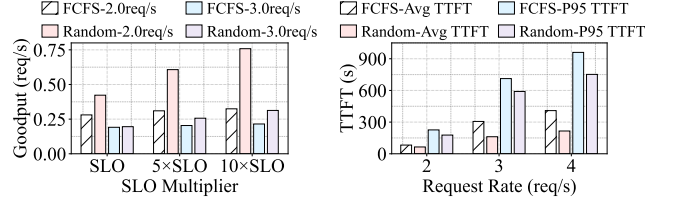
LLM inference services have become a dominant workload in modern data centers, motivating the design of advanced systems to improve overall efficiency.

To more efficiently handle arriving requests with varying sequence lengths, Orca [37] replaces request-level scheduling with iteration-level scheduling, forming batches before each iteration, allowing completed short requests to exit early, and admitting new requests. This design maximizes GPU parallelism and improves throughput and has been widely adopted in inference frameworks. Meanwhile, some efforts focus on improving GPU memory utilization. vLLM [21] introduces PagedAttention, which partitions GPU memory into fixed-size blocks and allocates them on demand. This avoids pre-allocating large memory regions and greatly reduces fragmentation, enhancing memory efficiency and inference performance. Additionally, some works optimize prefill and decode stages, such as chunked prefill [2] and prefill–decode separation [16, 42]. Other approaches explore offloading the KV cache to CPU memory or SSD storage [17, 18, 32] to alleviate GPU memory pressure.

While prior works adopt a single context (KV cache) handling policy during external calls in augmented LLM inference, InferCept [1] advances these approaches by dynamically selecting among *Preserve*, *Discard*, or *Swap* context handling policies based on the external call duration and context length:

- *Preserve*: The KV cache remains in GPU memory during the call, and decoding resumes once the response returns.
- *Discard*: The KV cache is discarded, and recomputation is required after the response returns.
- *Swap*: The KV cache is swapped to CPU memory, then moved back to GPU memory once the response returns.

Since each policy results in different memory waste, this



(a) Effective throughput (req/s).

(b) TTFT (s).

Figure 4: Effective throughput (req/s) and TTFT (s) with FCFS and random scheduling under different request rates.

adaptive design avoids inefficiently relying on a single policy and further reduces memory waste and inference latency.

3 Motivation

We focus on maximizing effective throughput under SLO constraints in augmented LLM inference services, as it directly impacts user experience. However, existing inference systems that rely on FCFS scheduling and static batch token limit struggle to meet this requirement. This motivates a systematic empirical investigation of current challenges and potential opportunities.

3.1 Rigid FCFS Scheduling Policy

Challenge 1: FCFS scheduling increases queuing delay and reduces effective throughput. Current inference systems typically adopt an FCFS scheduling, batching requests by arrival order without considering variations in input or output lengths. As a result, long requests block shorter ones, causing severe HOL blocking, higher queuing delays, and degraded throughput. In augmented LLM inference, unawareness of call return length worsens the problem. Specifically, early-arriving long requests with large token returns require substantial KV computation and memory footprint, blocking subsequent short requests and aggravating the HoL issue.

We use random scheduling to shuffle the request order and compare it with FCFS scheduling. We apply these scheduling policies on InferCept, running with OPT-13B on an NVIDIA H800 GPU, and using the merged augmented LLM dataset with Poisson arrivals. Following prior work [12, 35], we set the SLOs to a TTFT of 1s and an average token latency of 10× the iteration time.

As shown in Figure 4a, random scheduling consistently achieves higher effective throughput than FCFS across different loads. This indicates that FCFS batches requests strictly by arrival order and causes HoL blocking, leading to throughput degradation. In contrast, random scheduling breaks this rigid order, alleviating the HoL issue to some extent and thus achieving higher throughput. Meanwhile, Figure 4b illustrates that random scheduling yields lower queuing latency than FCFS under both load conditions. This occurs because re-ordering allows short requests to complete ahead of long ones, thereby reducing the queuing delays for some requests. As

Table 1: Effective throughput (req/s) with different max batch tokens, request rates, models, and GPUs.

Max batch tokens	100	500	1000	1500	2000
2.0req/s, GPT-J-6B, 4090 GPU	0.29	0.41	0.25	0.11	0.10
4.0req/s, OPT-13B, H800 GPU	0.01	0.16	0.18	0.22	0.19

a result, more requests meet the SLO constraints, consistent with the effective throughput results in Figure 4a.

However, random scheduling only coarsely shuffles the request order, providing limited improvement in throughput, while TTFT and tail latency remain high. This suggests that more fine-grained scheduling decisions are needed to better adapt to request features and system status, thereby achieving optimal performance.

Opportunity 1: Augmented LLM inference requires fine-grained scheduling to optimize request ordering, reducing queueing latency and enhancing effective throughput.

3.2 Fixed Batch Token Limit

Challenge 2: Fix batch token limit restricts throughput improvement. The batch token limit determines the maximum number of tokens processed in a single forward iteration. If the batch token limit is too small, each iteration can process only a few requests, and overall throughput remains low. Conversely, if the limit is set too large and exceeds GPU capacity, it leads to intensified resource contention. The GPU memory occupied by previously generated KV caches will be evicted, requiring additional recomputation, which in turn degrades the overall inference efficiency.

Building on the configuration in §3.1, we additionally run GPT-J-6B on an NVIDIA 4090 GPU to evaluate the effective throughput with different statically configured batch token limits. As shown in the Table 1, both excessively small and overly large limits degrade effective throughput. Moreover, the optimal token limit varies across hardware conditions and workload levels.

Opportunity 2: Dynamically adapting the batch token limit to real-time load and hardware status is essential for maximizing effective throughput.

3.3 Analysis of Augmented LLM Inference

We perform a detailed analysis on two augmented LLM datasets, including the Merge dataset from InferCept and the ToolBench dataset from ToolLLM [28]. Figure 5 illustrates the significant variations in request input, output, and external call (API) return lengths of requests. In particular, API returned tokens impose both high computational and memory demands during inference, as they require computing new

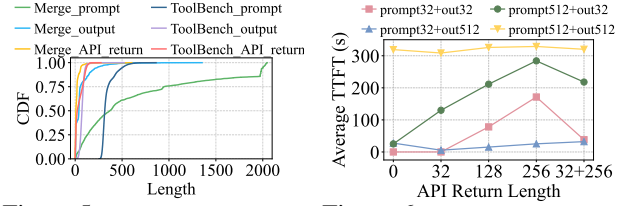


Figure 5: Input & output & API return length distribution. Figure 6: TTFT (s) with different API return lengths.

KVs for the returned tokens while relying on the KV cache of the preceding context.

We conduct experiments with different input, output, and API return lengths to evaluate system performance. As shown in Table 2, varying API return lengths result in distinct goodput performance. Larger API return lengths and mixing different API return lengths generally tend to reduce throughput. This underscores that API return length is a key factor influencing the system’s effective throughput. Figure 6 further presents the TTFT under different API return lengths. As the API return length increases, TTFT rises accordingly, suggesting that requests with large API return lengths require careful scheduling to mitigate the latency challenge.

Some prior works use output or total length to guide scheduling [10, 19, 31]. However, in augmented LLM inference, relying solely on total length is suboptimal, as it fails to accurately reflect the actual processing time. For example, even when Request 2 has a longer total length than Request 1 ($T_{l,2} > T_{l,1}$), it may still complete earlier ($T_{l,2} < T_{l,1}$) if their API return lengths difference that meets certain conditions. A simple derivation is provided below, with symbol definitions listed in Table 5 (Appendix A).

Proposition 1 (Longer request can finish earlier). *For request i , let the total length be $T_{l,i} = G_{l,i} + A_{l,i}$, where $G_{l,i}$ and $A_{l,i}$ denote the generation length and API return length, respectively. Let N_{\max} denote the maximum number of tokens processed per iteration, and I_t is the iteration time. The total service time $T_{l,i}$ is:*

$$T_{l,i} = G_{l,i} I_t + \frac{A_{l,i}}{N_{\max}} I_t = I_t \left(G_{l,i} + \frac{A_{l,i}}{N_{\max}} \right). \quad (1)$$

When $T_{l,2} > T_{l,1}$ and $T_{l,1} > T_{l,2}$ hold simultaneously, the necessary and sufficient condition is

$$T_{l,2} - T_{l,1} < \left(1 - \frac{1}{N_{\max}} \right) (A_{l,2} - A_{l,1}). \quad (2)$$

The proposition shows that a longer request can still finish earlier when the difference in API return length is sufficiently large relative to the total length difference.

In addition to return length, the context handling policies (e.g., *Preserve*, *Discard*, and *Swap*) during external calls also impact system performance. Different policies result in varying levels of memory overhead and consequently affect inference efficiency.

Table 2: Effective throughput (req/s) comparison with different API return length, prompt, and output lengths (token).

Prompt length + output length	32+32	32+512	512+32	512+512
API return 0	3.78	0.16	0.48	0.078
API return 32	3.71	0.24	0.23	0.070
API return 256	0.22	0.43	0.13	0.071
API return 32+256	0.45	0.35	0.15	0.068

Opportunity 3: External call characteristics should be incorporated into fine-grained scheduling to improve scheduling efficiency and overall system performance.

Insight and summary: Augmented LLM inference systems must consider not only overall workload, but also request specific external call features. These factors should guide the design of fine-grained scheduling and the dynamic setting of batch token limit that adapt to real-time load and system capacity, thereby reducing queuing delays and improving effective throughput.

4 Design

In this section, we present the core design of *AugServe*, which integrates a two-stage scheduling strategy and a dynamic token-level batching mechanism. The overall goal is to mitigate HoL blocking, reduce TTFT, and improve effective throughput.

4.1 Design Overview

AugServe consists of three modules: (1) Prediction module: estimates the output length range and API call duration from the request input and call type, providing prior signals to guide context handling policy selection and assist scheduling. (2) Scheduling module: computes scheduling values based on context handling policy and request features. To avoid error amplification and improve robustness, we adopt a two-stage design: (i) initially relying on predictions, (ii) while runtime feedback dynamically corrects priorities to ensure efficient and fair request ordering. (3) Dynamic token batching module: continuously monitors runtime load and resource usage to adaptively adjust the batch token limit with bounded constraints, ensuring stability while maintaining high throughput under fluctuating workloads. Together, these modules form a unified framework that reduces queueing delay, and maximizes effective throughput across diverse augmented LLM workloads.

4.2 Prediction of Request Characteristics

Efficient scheduling requires knowledge of the request output length, which is unknown before decoding. Following prior studies on output length prediction, we fine-tune a lightweight BERT-base-uncased model to estimate both the output length range and the API call duration. With only millions of parameters, the model provides fast predictions with negligi-

ble overhead, enabling seamless integration into the serving pipeline. For output length, we discretize ranges into buckets and formulate prediction as classification, a design shown to outperform direct regression [16, 19]. For API call duration, we adopt a regression approach leveraging observed time distributions across API types. We train and evaluate the model on the Merge and ToolBench datasets with 70/30 and 60/40 splits, respectively. Our model achieves 85% accuracy on ToolBench and 65% on Merge for output length prediction, and the mean squared error for API call time is about 5s and 0.4s. These levels are sufficient to support our scheduling strategy, and further accuracy optimization is left to future work.

4.3 Adaptive Two-Stage Scheduling Strategy

In augmented LLM inference services, request scheduling must cope with highly heterogeneous characteristics, including input length, output length, API call duration, and return length. A single-stage scheduler typically ranks requests at admission using predicted lengths or response times, but such static decisions tend to amplify prediction errors. For instance, if a long request is misclassified as a short one, placing at the head of the queue, discarding its context during API invocation, and recomputing upon return, leading to excessive GPU memory consumption and blocking subsequent requests, which is an instance of the HoL problem. Without a mechanism for runtime correction, such errors will accumulate, sharply increasing queueing latency and reducing throughput.

Therefore, an effective scheduling framework must combine predictive signals with adaptive correction during execution. Guided by this principle, we introduce a two-stage scheduling value estimation that evaluates and prioritizes requests separately in the pre-invocation and post-invocation phases, thereby integrating predictive foresight with runtime adaptivity.

Stage I: Predictive value estimation. When a request arrives, the system computes a provisional scheduling value representing the expected system cost of the request based on predictive features, including output length range, API call duration, return length, and context handling policy. By sorting requests according to this scheduling value, the system can prioritize those requests with lower expected costs and faster completion, thereby mitigating HoL blocking caused by long requests occupying the front of the requests queue.

Before request i enters the waiting queue, we first estimate its context handling policy $\hat{S}_i \in \{\text{Preserve}, \text{Discard}, \text{Swap}\}$ for the external call. Following InferCept, we choose a handling policy by minimizing the waiting-phase cost in terms of memory waste (Equations 4-8). The definitions of all symbols are listed in Table 5 in Appendix A. Here, T_i^{INT} denotes the duration of API call invocation, M is the context memory footprint per token, C_i means the context length, and T^{fwd} is the processing time of one forward iteration. The memory waste

of each handling policy, denoted as $\text{Waste}_i^{\text{policy}}$, is computed as follows:

$$\text{Waste}_i^{\text{Preserve}} = T_i^{\text{INT}} \cdot C_i \cdot M, \quad (4)$$

$$\text{Waste}_i^{\text{Discard}} = T^{\text{fwd}}(C_i) \cdot C_i \cdot M + T^{\text{fwd}}(C_i) \cdot C_{\text{other}} \cdot M, \quad (5)$$

$$\text{Waste}_i^{\text{Swap}} = 2 \cdot T^{\text{swap}}(C_i) \cdot N_{\text{max}}^{\text{fwd}} \cdot M, \quad (6)$$

$$\hat{S}_i = \text{policy} \in \{\text{Preserve}, \text{Discard}, \text{Swap}\}, \quad (7)$$

$$\text{Waste}_i^{\hat{S}_i} = \min(\text{Waste}_i^{\text{Preserve}}, \text{Waste}_i^{\text{Discard}}, \text{Waste}_i^{\text{Swap}}). \quad (8)$$

After selecting the context handling policy \hat{S}_i , we estimate the predicted scheduling value V_i accordingly. Specifically, we compute the system cost of request i across phases, including the prefill stage, the generation stage, and the memory residency during API call invocation. Under *Discard* and *Swap*, the request will release its context memory upon invocation, whereas under *Preserve* it remains allocated throughout. Since future rounds are hard to anticipate, the scheduling value V_i of *Preserve* is approximated using the system cost before the invocation returns.

Let Cost_i denote the cost of request i in a given phase. Here, L_i^{pre} represents the actual input length, \hat{L}_i^{out} is the predicted output length, \hat{T}_i^{api} is the predicted API invocation duration, $N_{\text{max}}^{\text{fwd}}$ and $S_{\text{out}}^{\text{fwd}}$ denote the maximum number of tokens processed per forward iteration, and the maximum number of tokens swapped out to CPU memory per iteration, respectively. The system cost for each phase is computed as follows:

$$\text{Cost}_i^{\text{prefill}} = \frac{1}{2} M \cdot \frac{(L_i^{\text{pre}})^2}{N_{\text{max}}^{\text{fwd}}} \cdot T^{\text{fwd}}, \quad (9)$$

$$\text{Cost}_i^{\text{decode}} = M \cdot T^{\text{fwd}} \left(L_i^{\text{pre}} \cdot \hat{L}_i^{\text{out}} + \frac{1}{2} (\hat{L}_i^{\text{out}})^2 \right), \quad (10)$$

$$\text{Cost}_i^{\text{api}} = M \cdot (L_i^{\text{pre}} + \hat{L}_i^{\text{out}}) \cdot \hat{T}_i^{\text{api}}, \quad (11)$$

$$\text{Cost}_i^{\text{swap-out}} = \frac{1}{2} M \cdot \frac{(L_i^{\text{pre}} + \hat{L}_i^{\text{out}})^2}{S_{\text{out}}^{\text{fwd}}} \cdot T^{\text{fwd}}. \quad (12)$$

Next, the scheduling value is computed based on the selected policy \hat{S}_i . Each policy includes the costs of the prefill and decode phases. Besides, *Preserve* accounts for memory residency during the API invocation, while *Swap* incorporates the overhead of context swapping. The calculation is as follows:

$$V_{i,\text{Preserve}}^{(1)} = \text{Cost}_i^{\text{prefill}} + \text{Cost}_i^{\text{decode}} + \text{Cost}_i^{\text{api}}, \quad (13)$$

$$V_{i,\text{Discard}}^{(1)} = \text{Cost}_i^{\text{prefill}} + \text{Cost}_i^{\text{decode}}, \quad (14)$$

$$V_{i,\text{Swap}}^{(1)} = \text{Cost}_i^{\text{prefill}} + \text{Cost}_i^{\text{decode}} + \text{Cost}_i^{\text{swap-out}}. \quad (15)$$

The scheduling value obtained in Stage I, $V_{i,\hat{S}_i}^{(1)}$, is used as the basis for ranking requests in the waiting queue or before the first external API invocation. However, since prediction errors may accumulate and system states can change after invocation, Stage II is introduced to refine this value with runtime observations and corrections.

Stage II: Runtime correction and re-prioritization. Although Stage I provides a prediction-based scheduling value

$V_{i,\hat{S}_i}^{(1)}$, its accuracy is limited by uncertainties in output length, API call time, and policy prediction. Such errors may accumulate, distorting priority ordering and increasing overall queuing delay. To mitigate this, we use runtime observations to replace predictions, correcting the scheduling value for each request. The corrected scheduling value $V_{i,\hat{S}_i}^{(2)}$ more accurately reflects the resource consumption of request i and serves for re-prioritization after invocation.

We present the system cost formulations after incorporating the actual return lengths of API calls, covering the context swap-in phase, the recomputation phase, the processing of API returned tokens, and the subsequent generation phase. After the call returns, the request re-enters the system with updated input information, which enables us to predict the output length and new call features of the new round. Here, L_i^{total} denotes the total length processed before the call, and \tilde{L}_i^{ret} denotes the actual return length of the call.

$$\text{Cost}_i^{\text{swap-in}} = \frac{1}{2} M \cdot \frac{(L_i^{\text{total}})^2}{S_{\text{in}}^{\text{fwd}}} \cdot T^{\text{fwd}}, \quad (16)$$

$$\text{Cost}_i^{\text{recompute}} = \frac{1}{2} M \cdot \frac{(L_i^{\text{total}})^2}{N_{\text{max}}^{\text{fwd}}} \cdot T^{\text{fwd}}, \quad (17)$$

$$\text{Cost}_i^{\text{pro-api}} = M \cdot \frac{T^{\text{fwd}}}{N_{\text{max}}^{\text{fwd}}} \left(L_i^{\text{total}} \cdot \tilde{L}_i^{\text{ret}} + \frac{1}{2} (\tilde{L}_i^{\text{ret}})^2 \right), \quad (18)$$

$$\text{Cost}_i^{\text{decode-post}} = M \cdot T^{\text{fwd}} \left((L_i^{\text{total}} + \tilde{L}_i^{\text{ret}}) \cdot \hat{L}_i^{\text{out,next}} + \frac{1}{2} (\hat{L}_i^{\text{out,next}})^2 \right). \quad (19)$$

The scheduling value is then determined according to the context handling policy \hat{S}_i applied during invocation.

$$V_{i,\text{Preserve}}^{(2)} = \text{Cost}_i^{\text{pro-api}} + \text{Cost}_i^{\text{decode-post}}, \quad (20)$$

$$V_{i,\text{Swap}}^{(2)} = \text{Cost}_i^{\text{swap-in}} + \text{Cost}_i^{\text{pro-api}} + \text{Cost}_i^{\text{decode-post}}, \quad (21)$$

$$V_{i,\text{Discard}}^{(2)} = \text{Cost}_i^{\text{recompute}} + \text{Cost}_i^{\text{pro-api}} + \text{Cost}_i^{\text{decode-post}}. \quad (22)$$

Building on the Stage II scheduling value $V_{i,\hat{S}_i}^{(2)}$, we incorporate the potential context handling policy in the new round to obtain the final scheduling value V_i^{final} . If the next round adopts *Swap*, the additional cost of swapping out context is included; if it adopts *Preserve*, the memory footprint during the subsequent API invocation will be contained. In this way, V_i^{final} provides a more comprehensive estimate of future resource consumption, serving as the basis for cross-round scheduling decisions.

$$V_{i,\text{Swap}}^{\text{final}} = V_{i,\hat{S}_i}^{(2)} + \frac{1}{2} M \cdot \frac{(L_i^{\text{total}} + \tilde{L}_i^{\text{ret}} + \hat{L}_i^{\text{out,next}})^2}{S_{\text{out}}^{\text{fwd}}} \cdot T^{\text{fwd}}, \quad (23)$$

$$V_{i,\text{Preserve}}^{\text{final}} = V_{i,\hat{S}_i}^{(2)} + M \cdot (L_i^{\text{total}} + \tilde{L}_i^{\text{ret}} + \hat{L}_i^{\text{out,next}}) \cdot \hat{T}_i^{\text{api,next}}, \quad (24)$$

$$V_{i,\text{Discard}}^{\text{final}} = V_{i,\hat{S}_i}^{(2)}. \quad (25)$$

Anti-starvation adjustment. On top of the final scheduling value V_i^{final} , we incorporate an anti-starvation term to ensure

that long-waiting requests gradually gain higher priority. The waiting time is measured as the difference between the current time and the last scheduling time, while the coefficient α controls the trade-off between fairness and throughput:

$$V_i^{\text{sched}} = V_i^{\text{final}} + \alpha \cdot (\text{now} - \text{last_schedule_time}_i). \quad (26)$$

In summary, we designed an adaptive scheduling strategy that integrates prediction-driven scheduling value estimation (Stage I), runtime correction with real-time information (Stage II), and an anti-starvation mechanism. The overall algorithm details are provided in Appendix A. This design enables the system to dynamically balance adaptability and fairness, ensuring high throughput and stable latency performance in augmented LLM inference services.

4.4 Dynamic Token Batching

Existing systems often use a fixed batch token limit to safeguard GPU memory, but this static approach limits throughput. To address this, we design a dynamic batch token limit mechanism that adjusts the maximum number of tokens processed per iteration according to runtime resource availability.

Specifically, we monitor two key quantities: (i) free GPU memory and (ii) context memory of paused requests. We configure the paused memory can be preempted by active requests, so the sum of the two parts is considered as the available capacity. Based on this, we calculate the current memory usage of each component, denoted by G^{part} , as follows:

$$G_{\text{kv}}^{\text{active}}(t) = M \cdot \sum_{i \in \text{running}} L_i^{\text{total}}, \quad (27)$$

$$G_{\text{kv}}^{\text{paused}}(t) = M \cdot \sum_{j \in \text{paused}} L_j^{\text{total}}, \quad (28)$$

$$G_{\text{fixed}} = G_{\text{model}} + G_{\text{runtime}} + G_{\text{safety}}, \quad G_{\text{safety}} > 0. \quad (29)$$

$$G_{\text{free}}(t) = G_{\text{total}} - G_{\text{fixed}} - G_{\text{kv}}^{\text{active}}(t) - G_{\text{kv}}^{\text{paused}}(t). \quad (30)$$

$$G_{\text{avail}}(t) = G_{\text{free}}(t) + \gamma \cdot G_{\text{kv}}^{\text{paused}}(t), \quad \gamma \in [0, 1], \text{ default } \gamma = 1. \quad (31)$$

$$\text{token_budget}(t) = \left\lfloor \frac{G_{\text{avail}}(t)}{M} \right\rfloor. \quad (32)$$

To prevent transient fluctuations in available GPU memory from causing excessive token budget expansion and memory overload, we add interval constraints. We first determine an appropriate reference upper limit $\text{target}_{\text{max}}$ through offline profiling. At runtime, the dynamic token limit is bounded within $[\beta_{\text{low}} \cdot \text{target}_{\text{max}}, \beta_{\text{high}} \cdot \text{target}_{\text{max}}]$, where β_{low} and β_{high} serve as smoothing parameters. This ensures flexible scaling under real-time conditions while avoiding over-adjustments from short-term memory variations.

To sum up, this mechanism enhances overall throughput and improves scheduling efficiency.

5 Evaluation

We evaluate our approach and baselines across different hardware, models, and datasets. We first analyze end-to-end performance, including effective throughput, TTFT, and normalized latency, then conduct sensitivity and robustness studies, and finally perform ablation experiments to assess each component's effects.

5.1 Experiment Setup

Environment and models. Our experiments are conducted on diverse hardware platforms to demonstrate the generality of our system. We run GPT-J-6B on an NVIDIA RTX 4090 GPU with 24GB memory, and OPT-13B on either an NVIDIA H800 GPU with 80GB memory or two NVIDIA A100 GPUs with 40GB memory each.

Datasets. To assess the effectiveness of *AugServe* in augmented LLM inference, we adopt two representative datasets: (i) a merged dataset by integrating six categories of augmented LLM tasks used in InferCept. We refer to this dataset as "Merge" throughout the paper. And (ii) ToolBench, provided by ToolLLM [28], which contains thousands of API calls spanning dozens of categories.

Workloads. We consider three types of workload generation: (W1) a Poisson arrival process, running for 30 minutes to simulate real-world random request streams; (W2) a fixed request count of 2k requests to evaluate system completion efficiency; and (W3) a Gamma arrival process, also running for 30 minutes, where the coefficient of variation (CV) is adjusted to control burstiness under the same average arrival rate, serving as a robustness test.

Baselines and metrics. We compare *AugServe* with vLLM and InferCept, focusing on performance under SLO constraints. For latency, we report normalized latency and TTFT. Normalized latency is defined as the each request's end-to-end latency divided by its generated length, and TTFT captures the time to generate the first token and includes queuing delay. For throughput, we measure Goodput and SLOs Attainment. Goodput is the number of SLO-satisfying requests completed per unit time. SLOs Attainment is the fraction of completed requests that meet SLOs, reflecting service quality. Following prior work, we set SLOs as TTFT < 1s and normalized latency < 10× iteration time.

5.2 End-to-End Performance

We evaluate *AugServe* against vLLM and InferCept by measuring effective throughput, TTFT, and normalized latency on Merge and ToolBench under W1 workload with GPT-J-6B and OPT-13B on different GPUs. The results demonstrate that *AugServe* significantly boosts effective throughput and also reduces TTFT and normalized latency, highlighting its advantages in augmented LLM inference.

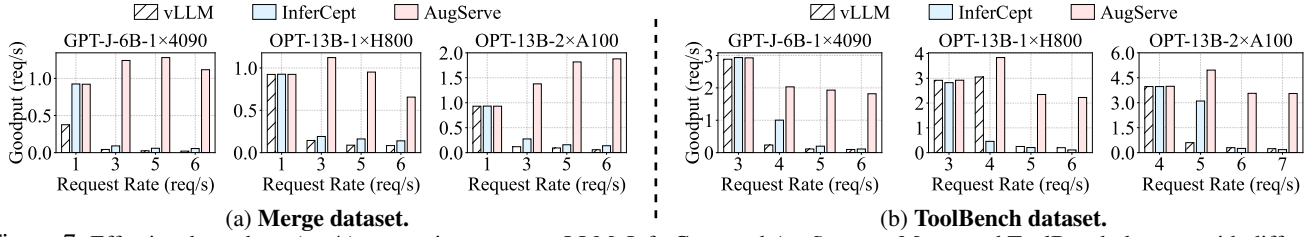


Figure 7: Effective throughput (req/s) comparison among vLLM, InferCept, and *AugServe* on Merge and ToolBench datasets with different models and GPUs. Higher is better.

5.2.1 Effective Throughput

Figure 7 presents the effective throughput of *AugServe* and the baselines across different hardware configurations and request rates. Across all load levels, *AugServe* consistently achieves the highest goodput. On the Merge dataset, corresponding to the three experimental environments in Figure 7, *AugServe* delivers average 33.2 \times , 5.9 \times , and 15.0 \times higher effective throughput than vLLM, and 12.9 \times , 3.4 \times , and 6.8 \times higher than InferCept. On ToolBench, similar improvements are observed. For example, at a load of 5.0 req/s on the H800 with ToolBench, the goodput of vLLM and InferCept is only 0.25req/s and 0.21req/s, while *AugServe* maintains a high level of approximately 2.35 req/s.

The fundamental reason for this discrepancy is that, as load increases, FCFS scheduling exacerbates the HoL blocking. Furthermore, high concurrency intensifies GPU memory contention, triggering frequent KV swapping and recomputation. These factors together increase latency and cause a large number of requests to miss SLOs, resulting in the sharp throughput degradation of vLLM and InferCept. By contrast, *AugServe* alleviates HoL blocking by its two-stage adaptive scheduling, and adapts to varying loads via dynamic token batching, which avoids excessive recomputation and resource waste. As a result, *AugServe* sustains significantly higher effective throughput across all hardware and loads, with its advantage particularly evident on memory-constrained consumer GPUs. For instance, on the RTX 4090 GPU, *AugServe* achieves more than 10 \times higher goodput than both vLLM and InferCept. We also present the effective throughput at 5 \times SLOs in Appendix B to further validate the stability and performance of *AugServe*.

Summary. *AugServe* outperforms vLLM and InferCept, achieving substantially higher effective throughput.

5.2.2 TTFT

TTFT is a critical factor for effective throughput, as failing to meet the TTFT SLO causes a large number of requests to be treated as invalid, leading to a significant drop in goodput. Figure 8 compares the average TTFT of *AugServe* with vLLM and InferCept under different configurations. In all scenarios, *AugServe* consistently achieves lower TTFT than the baselines, with reductions of up to 96.3% and 95.0%. As the load increases, TTFT rises across all systems, but *AugServe* main-

tains excellent performance. For example, at 5.0 req/s with Merge on H800, the average TTFT of *AugServe* is reduced by 90.8% compared to InferCept and 90.5% compared to vLLM. This reduction in TTFT enables more requests to complete within the SLOs, sustaining higher effective throughput. We also present the comparison of P95 TTFT (the 95th-percentile TTFT) in Appendix B, which evaluates the system’s tail latency.

Summary. *AugServe* markedly reduces TTFT, indicating lower queuing delays and more efficient request scheduling.

5.2.3 Normalization Latency

We further evaluate normalized latency, defined as end-to-end latency divided by output length. This metric reflects the average token response efficiency and removes the bias of varying output lengths, allowing fairer comparison across requests. As shown in Figure 9, normalized latency increases for all systems as the load grows, but the growth of *AugServe* is much slower than that of InferCept and vLLM. For example, at 5.0 req/s on the ToolBench dataset and H800 GPU, the average normalized latency of *AugServe* is reduced by 57.6% and 80.3% compared to InferCept and vLLM, respectively. Overall, *AugServe* achieves 80.3% and 62.7% lower normalized latency than vLLM and InferCept, indicating higher token generation efficiency. Combined with TTFT reductions, the lower normalized latency demonstrates *AugServe*’s distinct advantages in both request-level and token-level efficiency. Similarly, the results of P95 normalized latency and time-per-output-token (TPOT) are presented in Appendix B to supplement the analysis of tail latency and decoding efficiency.

Summary. *AugServe* consistently achieves the lowest normalized latency, reflecting higher per-token efficiency.

5.3 Sensitivity and Robustness

In this section, we fix the workload to 2k requests (W2 workload) to compare the performance of different systems under the same task volume. We report effective throughput and SLOs attainment to evaluate completion efficiency and service quality.

Table 3 presents the effective throughput when processing 2k requests with OPT-13B on an H800 GPU. On the Merge dataset, at 3.0 req/s, *AugServe* achieves a goodput of 0.57 req/s, two to three times higher than vLLM (0.15 req/s) and

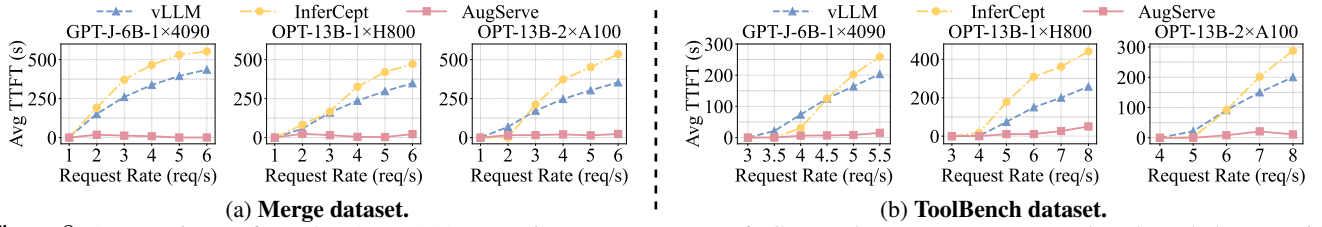


Figure 8: Average time-to-first-token (TTFT) (s) comparison among vLLM, InferCept, and *AugServe* on Merge and ToolBench datasets with different models and GPUs. Lower right is better, i.e., shorter response time and queueing time.

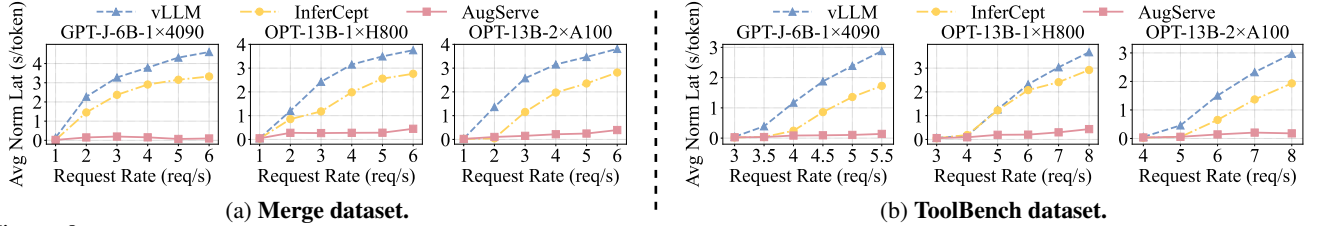


Figure 9: Average token Latency (s/token) comparison among vLLM, InferCept, and *AugServe* on Merge and ToolBench datasets with different models and GPUs. Lower right is better, i.e., sustains higher serving load.

Table 3: Effective throughput (req/s) comparison of vLLM, InferCept, and *AugServe* on Merge and ToolBench datasets under different request rates (req/s) with OPT-13B and an H800 GPU.

Datasets	Merge dataset			ToolBench dataset		
Request rate	2.0	3.0	4.0	4.0	5.0	6.0
vLLM	0.22	0.15	0.11	1.09	0.25	0.19
InferCept	0.27	0.21	0.16	0.31	0.16	0.10
<i>AugServe</i>	0.60	0.57	0.51	1.11	0.71	0.56

Table 4: Time breakdown for serving requests with *AugServe* on Merge and ToolBench datasets with OPT-13B and an H800 GPU.

Breakdown	Predict	Queueing	Execute
Merge-3.0req/s	0.55%	10.88%	88.57%
ToolBench-5.0req/s	0.14%	8.57%	91.29%

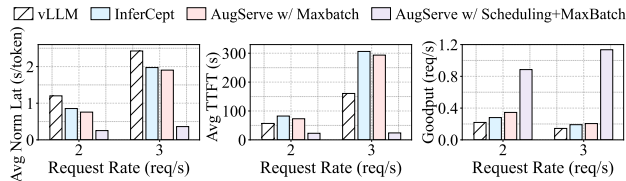


Figure 10: Breakdown of *AugServe* components with Merge dataset, OPT-13B, and an H800 GPU.

InferCept (0.21 req/s). On ToolBench, at a load of 5.0 req/s, *AugServe* still sustains 0.71 req/s, while vLLM and InferCept fall to 0.25 req/s and 0.16 req/s, respectively. Overall, across both datasets and all load levels, *AugServe* consistently delivers higher goodput than vLLM and InferCept, and maintains stable performance even under heavy load. We also report the corresponding SLOs attainment under the same experimental setting in Appendix B. Otherwise, We also assess the robustness of *AugServe* and the baselines under varying burstiness in request arrivals, which is detailed in Appendix B.

Summary. Under the 2k-request setting, *AugServe* achieves higher effective throughput than vLLM and InferCept, confirming superior efficiency and service quality.

5.4 Ablation Study

To further understand the effectiveness of the *AugServe* design, we conduct an ablation study by breaking down its core

components. Specifically, we first add dynamic token batching (*AugServe* w/ MaxBatch in Figure 10) to evaluate the throughput improvement. We then introduce a two-stage scheduling strategy and compare it against vLLM and InferCept, both of which use FCFS scheduling to assess additional performance improvements. The experiments used the Merge dataset, the OPT-13B model, and an H800 GPU.

Figure 10 presents the results on key performance metrics. First, the introduction of dynamic token batching improves effective throughput. For example, with a load is 2.0 req/s, this design increases vLLM’s 0.22 req/s and InferCept’s 0.28 req/s to 0.35 req/s. This shows that the dynamic batching mechanism can effectively adapt to runtime resource conditions and enhance overall efficiency. Moreover, with the addition of two-stage scheduling, effective throughput is further significantly improved, and latency is obviously reduced. This is because FCFS strictly follows arrival order, while our scheduling strategy adapts to request features, thereby enhancing overall efficiency.

Furthermore, Table 4 shows the breakdown of request completion time in *AugServe*, where the prediction module accounts for less than 1% of the total, making its overhead negligible.

Summary. The ablation study shows that dynamic batching helps improve goodput. Furthermore, introducing two-stage scheduling significantly reduces TTFT and further boosts effective throughput, confirming the complementary benefits of both components.

6 Related Work

Memory optimizations. vLLM [21] improves GPU memory utilization with PageAttention, allocating memory in fixed-size blocks and gradually assigning them, reducing fragmentation and memory waste. InferCept [1] proposes a dynamic context handling strategy during augmented LLM inference pauses, selectively swapping KV cache to CPU memory to minimize memory waste. Sarathi [2] employs chunked prefill, splitting the input into blocks and processing them together with decoding to maximize resource utilization. FlexGen [32] and FlashGen [18] optimize KV cache management by offloading data to CPU memory or SSDs to boost throughput. These memory optimization techniques, including PageAttention, dynamic context handling, and chunked prefill, are already integrated into *AugServe* to enhance performance.

Scheduling. Recent research has made efforts in optimizing requests scheduling. For instance, Orca [37] uses iteration-level batching to leverage GPU parallelism, and FastServe [35] employs preemptive time-slicing to reduce completion times. Other methods [10, 16, 19, 30, 31, 41] predict output lengths for near-shortest-job-first (SJF) scheduling to minimize queuing delays. However, these approaches fail to address the unique characteristics of augmented LLM inference, such as API call return length, making them less suitable for augmented LLM. *AugServe* overcomes these limitations with an adaptive two-stage scheduling strategy that dynamically adjusts to key features of augmented LLM inference, for efficient request scheduling and improved throughput.

7 Conclusion

This paper proposes *AugServe* to optimize inference efficiency for augmented LLM inference services. The core of *AugServe* is an adaptive request scheduling strategy and dynamic token batching. *AugServe* introduces two-stage scheduling decisions and runtime corrections, tailored to the unique features of augmented LLM inference and varying request demands. Additionally, *AugServe* dynamically adjusts the batch token limit based on real-time conditions, efficiently adapting to workload variations. Combining these two advantages, *AugServe* reduces overall queuing delays and significantly improves effective throughput. Experiments demonstrate the high efficiency and stability of *AugServe*.

References

- [1] Reyna Abhyankar, Zijian He, Vikranth Srivatsa, Hao Zhang, and Yiyang Zhang. Infercept: efficient intercept support for augmented large language model inference. In *Proceedings of the 41st International Conference on Machine Learning, ICML’24*. JMLR.org, 2024.
- [2] Amey Agrawal, Nitin Kedia, Ashish Panwar, Jayashree Mohan, Nipun Kwatra, Bhargav Gulavani, Alexey Tumanov, and Ramachandran Ramjee. Taming {Throughput-Latency} tradeoff in {LLM} inference with {Sarathi-Serve}. In *18th USENIX Symposium on Operating Systems Design and Implementation (OSDI 24)*, pages 117–134, 2024.
- [3] Anonymous. Revisiting service level objectives and system level metrics in large language model serving. In *Submitted to ACL Rolling Review - February 2025*, 2025. under review.
- [4] Anthropic. Model context protocol (mcp). <https://modelcontextprotocol.io>, 2024.
- [5] Nuo Chen, Hongguang Li, Baoyuan Wang, and Jia Li. From good to great: Improving math reasoning with tool-augmented interleaf prompting. In Bhavana Dalvi Mishra, Greg Durrett, Peter Jansen, Ben Lipkin, Danilo Neves Ribeiro, Lionel Wong, Xi Ye, and Wenting Zhao, editors, *Proceedings of the 2nd Workshop on Natural Language Reasoning and Structured Explanations (@ACL 2024)*, pages 64–79, Bangkok, Thailand, August 2024. Association for Computational Linguistics.
- [6] Sijia Chen, Yibo Wang, Yi-Feng Wu, Qingguo Chen, Zhao Xu, Weihua Luo, Kaifu Zhang, and Lijun Zhang. Advancing tool-augmented large language models: Integrating insights from errors in inference trees. *Advances in Neural Information Processing Systems*, 37:106555–106581, 2024.
- [7] Zhipeng Chen, Kun Zhou, Beichen Zhang, Zheng Gong, Wayne Xin Zhao, and Ji-Rong Wen. Chatcot: Tool-augmented chain-of-thought reasoning on chat-based large language models. *arXiv preprint arXiv:2305.14323*, 2023.
- [8] Sebastian Farquhar, Jannik Kossen, Lorenz Kuhn, and Yarin Gal. Detecting hallucinations in large language models using semantic entropy. *Nature*, 630(8017):625–630, 2024.
- [9] Xiang Fei, Xiawu Zheng, and Hao Feng. Mcp-zero: Proactive toolchain construction for llm agents from scratch. *arXiv preprint arXiv:2506.01056*, 2025.
- [10] Yichao Fu, Siqi Zhu, Runlong Su, Aurick Qiao, Ion Stoica, and Hao Zhang. Efficient llm scheduling by learning to rank. *Advances in Neural Information Processing Systems*, 37:59006–59029, 2024.
- [11] Anoushka Gade, Jorjeta G. Jetcheva, and Hardi Trivedi. It’s about time: Incorporating temporality in retrieval augmented language models. In *2025 IEEE Conference on Artificial Intelligence (CAI)*, pages 75–82, 2025.

- [12] Shihong Gao, Xin Zhang, Yanyan Shen, and Lei Chen. Apt-serve: Adaptive request scheduling on hybrid cache for scalable llm inference serving. *Proceedings of the ACM on Management of Data*, 3(3):1–28, 2025.
- [13] In Gim, Seung-seob Lee, and Lin Zhong. Asynchronous llm function calling. *arXiv preprint arXiv:2412.07017*, 2024.
- [14] HeounMo Go and SangHyun Park. A study on classification based concurrent api calls and optimal model combination for tool augmented llms for ai agent. *Scientific Reports*, 15(1):20579, 2025.
- [15] Shibo Hao, Tianyang Liu, Zhen Wang, and Zhiting Hu. Toolkengpt: Augmenting frozen language models with massive tools via tool embeddings. *Advances in neural information processing systems*, 36:45870–45894, 2023.
- [16] CunChen Hu, HeYang Huang, LiangLiang Xu, XuSheng Chen, Chenxi Wang, Jiang Xu, Shuang Chen, Hao Feng, Sa Wang, Yungang Bao, et al. Shuffleinfer: Disaggregate llm inference for mixed downstream workloads. *ACM Transactions on Architecture and Code Optimization*, 2025.
- [17] Yitao Hu, Xiulong Liu, Guotao Yang, Linxuan Li, Kai Zeng, Zhixin Zhao, Sheng Chen, Laiping Zhao, Wenxin Li, and Keqiu Li. Tightllm: Maximizing throughput for llm inference via adaptive offloading policy. *IEEE Transactions on Computers*, 2025.
- [18] Jinwoo Jeong and Jeongseob Ahn. Accelerating llm serving for multi-turn dialogues with efficient resource management. In *Proceedings of the 30th ACM International Conference on Architectural Support for Programming Languages and Operating Systems, Volume 2*, pages 1–15, 2025.
- [19] Yunho Jin, Chun-Feng Wu, David Brooks, and Gu-Yeon Wei. S3: increasing gpu utilization during generative inference for higher throughput. NIPS '23, Red Hook, NY, USA, 2023. Curran Associates Inc.
- [20] Srinivas Karthik, Panagiotis Sioulas, Ahana Pradhan, Raghunandan Subramanya, Ioannis Mytilinis, and Anastasia Ailamaki. Optimizing goodput through sharing for batch analytics with deadlines. In *EDBT*, pages 332–344, 2024.
- [21] Woosuk Kwon, Zhuohan Li, Siyuan Zhuang, Ying Sheng, Lianmin Zheng, Cody Hao Yu, Joseph Gonzalez, Hao Zhang, and Ion Stoica. Efficient memory management for large language model serving with pagedattention. In *Proceedings of the 29th symposium on operating systems principles*, pages 611–626, 2023.
- [22] Yining Lu, Haoping Yu, and Daniel Khashabi. Gear: Augmenting language models with generalizable and efficient tool resolution. *arXiv preprint arXiv:2307.08775*, 2023.
- [23] Grégoire Mialon, Roberto Dessì, Maria Lomeli, Christoforos Nalmpantis, Ram Pasunuru, Roberta Raileanu, Baptiste Rozière, Timo Schick, Jane Dwivedi-Yu, Asli Celikyilmaz, et al. Augmented language models: a survey. *arXiv preprint arXiv:2302.07842*, 2023.
- [24] OpenAI. Introducing function calling in chatgpt. <https://openai.com/blog/function-calling>, 2023.
- [25] Pratyush Patel, Esha Choukse, Chaojie Zhang, Aashaka Shah, Íñigo Goiri, Saeed Maleki, and Ricardo Bianchini. Splitwise: Efficient generative llm inference using phase splitting. In *Proceedings of the 51st Annual International Symposium on Computer Architecture, ISCA '24*, page 118–132. IEEE Press, 2025.
- [26] Zehan Qi, Xiao Liu, Iat Long Iong, Hanyu Lai, Xueqiao Sun, Jiadai Sun, Xinyue Yang, Yu Yang, Shuntian Yao, Wei Xu, Jie Tang, and Yuxiao Dong. WebRL: Training LLM web agents via self-evolving online curriculum reinforcement learning. In *The Thirteenth International Conference on Learning Representations*, 2025.
- [27] Yujia Qin, Shengding Hu, Yankai Lin, Weize Chen, Ning Ding, Ganqu Cui, Zheni Zeng, Xuanhe Zhou, Yufei Huang, Chaojun Xiao, et al. Tool learning with foundation models. *ACM Computing Surveys*, 57(4):1–40, 2024.
- [28] Yujia Qin, Shihao Liang, Yining Ye, Kunlun Zhu, Lan Yan, Yaxi Lu, Yankai Lin, Xin Cong, Xiangru Tang, Bill Qian, Sihan Zhao, Lauren Hong, Runchu Tian, Ruobing Xie, Jie Zhou, Mark Gerstein, dahai li, Zhiyuan Liu, and Maosong Sun. ToolLLM: Facilitating large language models to master 16000+ real-world APIs. In *The Twelfth International Conference on Learning Representations*, 2024.
- [29] Timo Schick, Jane Dwivedi-Yu, Roberto Dessì, Roberta Raileanu, Maria Lomeli, Eric Hambro, Luke Zettlemoyer, Nicola Cancedda, and Thomas Scialom. Toolformer: Language models can teach themselves to use tools. *Advances in Neural Information Processing Systems*, 36:68539–68551, 2023.
- [30] Rana Shahout, eran malach, Chunwei Liu, Weifan Jiang, Minlan Yu, and Michael Mitzenmacher. DON't STOP ME NOW: EMBEDDING BASED SCHEDULING FOR LLMS. In *The Thirteenth International Conference on Learning Representations*, 2025.

- [31] Rana Shahout, Cong Liang, Shiji Xin, Qianru Lao, Yong Cui, Minlan Yu, and Michael Mitzenmacher. Fast inference for augmented large language models. *arXiv preprint arXiv:2410.18248*, 2024.
- [32] Ying Sheng, Lianmin Zheng, Binhang Yuan, Zhuohan Li, Max Ryabinin, Beidi Chen, Percy Liang, Christopher Ré, Ion Stoica, and Ce Zhang. Flexgen: High-throughput generative inference of large language models with a single gpu. In *International Conference on Machine Learning*, pages 31094–31116. PMLR, 2023.
- [33] Weihang Su, Yichen Tang, Qingyao Ai, Zhijing Wu, and Yiqun Liu. Dragin: dynamic retrieval augmented generation based on the information needs of large language models. *arXiv preprint arXiv:2403.10081*, 2024.
- [34] B. Wang and A. Komatsuzaki. Gpt-j-6b: A 6 billion parameter autoregressive language model, 2021. Accessed: 2023-09-25.
- [35] Bingyang Wu, Yinmin Zhong, Zili Zhang, Shengyu Liu, Fangyue Liu, Yuanhang Sun, Gang Huang, Xuanzhe Liu, and Xin Jin. Fast distributed inference serving for large language models. *arXiv preprint arXiv:2305.05920*, 2023.
- [36] Bohan Yao and Vikas Yadav. A toolbox, not a hammer—multi-tag: Scaling math reasoning with multi-tool aggregation. *arXiv preprint arXiv:2507.18973*, 2025.
- [37] Gyeong-In Yu, Joo Seong Jeong, Geon-Woo Kim, Soojeong Kim, and Byung-Gon Chun. Orca: A distributed serving system for {Transformer-Based} generative models. In *16th USENIX Symposium on Operating Systems Design and Implementation (OSDI 22)*, pages 521–538, 2022.
- [38] Hong Zhang, Yupeng Tang, Anurag Khandelwal, and Ion Stoica. {SHEPHERD}: Serving {DNNs} in the wild. In *20th USENIX Symposium on Networked Systems Design and Implementation (NSDI 23)*, pages 787–808, 2023.
- [39] Susan Zhang, Stephen Roller, Naman Goyal, Mikel Artetxe, Moya Chen, Shuohui Chen, Christopher Dewan, Mona Diab, Xian Li, Xi Victoria Lin, et al. Opt: Open pre-trained transformer language models. *arXiv preprint arXiv:2205.01068*, 2022.
- [40] Yao Zhang, Zijian Ma, Yunpu Ma, Zhen Han, Yu Wu, and Volker Tresp. Webpilot: a versatile and autonomous multi-agent system for web task execution with strategic exploration. In *Proceedings of the Thirty-Ninth AAAI Conference on Artificial Intelligence and Thirty-Seventh Conference on Innovative Applications of Artificial Intelligence and Fifteenth Symposium on Educational Advances in Artificial Intelligence, AAAI’25/IAAI’25/EAAI’25*. AAAI Press, 2025.
- [41] Zangwei Zheng, Xiaozhe Ren, Fuzhao Xue, Yang Luo, Xin Jiang, and Yang You. Response length perception and sequence scheduling: an llm-empowered llm inference pipeline. In *Proceedings of the 37th International Conference on Neural Information Processing Systems, NIPS ’23*, Red Hook, NY, USA, 2023. Curran Associates Inc.
- [42] Yinmin Zhong, Shengyu Liu, Junda Chen, Jianbo Hu, Yibo Zhu, Xuanzhe Liu, Xin Jin, and Hao Zhang. {DistServe}: Disaggregating prefill and decoding for goodput-optimized large language model serving. In *18th USENIX Symposium on Operating Systems Design and Implementation (OSDI 24)*, pages 193–210, 2024.

Table 5: Notation and definitions of key symbols.

Symbol	Definition
$T_{l,i}$	Total length of request i (generate and API return)
$T_{t,i}$	Total processing time of request i
$G_{l,i}$	Generate length of request i
$A_{l,i}$	API return length of request i
N_{\max}^{fwd}	Maximum number of tokens processed per iteration
M	Per-token KV cache memory footprint
T_i^{INT}	API call duration of request i
C_i	Context length (tokens) before external API invocation
T^{fwd}	Processing time of one forward iteration
L_i^{pre}	Actual input length of request i (prefill tokens)
\hat{L}_i^{out}	Predicted output length of request i
\tilde{L}_i^{out}	Observed (true) output length of request i
\hat{T}_i^{api}	Predicted API invocation duration of request i
\tilde{L}_i^{ret}	Observed API return length of request i
L_i^{total}	Total length processed before API call of request i
S^{fwd}	Maximum number of tokens swapped per iteration
\hat{S}_i	Predicted context-handling policy for request i
\tilde{S}_i	Selected context-handling policy for request i
Cost_i	System cost of request i in a specific phase
$V_{i,\hat{S}_i}^{(1)}$	Stage I scheduling value of request i (prediction-based)
V_i^{final}	Stage II scheduling value of request i (runtime-corrected)
V_i^{sched}	Scheduling value with waiting time of request i
G_{kv}^{active}	Memory footprint of running requests
G_{kv}^{paused}	Memory footprint of paused requests
G_{kv}^{avail}	Available memory for new tokens

A Algorithm

Table 5 defines the symbols used in the paper’s equations. Algorithm 1 illustrates how *AugServe* employs a two-stage adaptive request scheduling strategy and dynamic token batching mechanism to perform scheduling in each iteration. Upon request arrival, the prediction module is invoked to estimate the external call time and output length, helping select an optimal context handling policy. This informs the calculation of the stage I scheduling value, which determines the initial order of requests (lines 2-9). After the actual call is completed, the scheduling value for stage II is updated based on the actual context handling policy and API return length, and the request is reinserted into the appropriate queue according to the chosen policy (lines 10-24). Additionally, the available GPU memory is used to update the batch token limit in each iteration, maintaining it within an optimal range to prevent extreme fluctuations (line 25-27). Finally, the requests are sorted based on their scheduling values (lines 28), and the batch is filled sequentially until it is full (lines 30-40) and processed in a forward pass.

B Performance

B.1 Evaluation of Robustness

To evaluate the robustness of *AugServe* and the two baseline systems under burst traffic, we use the Gamma distribution to simulate the request arrival process and the coefficient of variation (CV) to control the level of load fluctuation. Specifically, we fix different request rates in the two datasets with OPT-13B on an H800 GPU, then set various coefficients of variation to compare the effective throughput of several inference systems.

Table 6 presents a detailed goodput comparison. Across all datasets and load conditions, *AugServe* exhibits more stable performance compared to vLLM and InferCept. As shown in the table, as the burst request level increases, the efficiency of the inference system declines. For instance, under the Merge workload with a load of 2.0 req/s and CV = 1.5, the effective throughput of both vLLM and InferCept drops to approximately 0.1 req/s. However, *AugServe* maintains a stable 1.15 req/s, demonstrating excellent reliability.

Summary. *AugServe* enhances effective throughput while ensuring superior system stability.

B.2 Effective Throughput of Different Metrics

B.2.1 Workloads with Fixed Requests

Table 7 reports the SLO attainment under the same experimental conditions as in §5.3, with a fixed total service request count of 2k and varying request rates. This metric reflects the qualification rate at which the inference system successfully completes requests under SLO constraints. As the load

Algorithm 1: *AugServe* Scheduler

Input: Request queues: running, swapped, waiting_resume, waiting_new, paused;
predictor Pred; waiting parameter α ; token parameter β ; token limit N_{\max}

```

1 while True do
    // (1) Stage-I scheduling value
2   foreach  $r \in arrivals$  do
3     ( $pre\_call\_duration_r, pre\_generate_r$ )  $\leftarrow$  Pred( $r$ )
4     compute  $Waste_r^{Preserve}, Waste_r^{Discard}, Waste_r^{Swap}$ 
5      $r.pre\_policy \leftarrow \arg \min\{Waste_r\}$ 
6      $V_{r,pre\_policy}^{(1)} \leftarrow Cost_r^{phases}$  by (9)-(15)
7      $r.stage1\_sched\_value \leftarrow V_{r,pre\_policy}^{(1)}$ 
8     waiting_new.push( $r$ )
9   end
    // (2) Stage-II scheduling value
10  foreach  $(r, S) \in paused$  do
11    if  $r.apiFinished()$  then
12      update  $V_r^{(2)} \leftarrow S$  & API return length by
        (16)-(22)
13      if  $S = Preserve$  then
14        running.push( $r$ )
15      end
16      else if  $S = Swap$  then
17        swapped.push( $r$ )
18      end
19      else
20        waiting_resume.push( $r$ ) // Discard
21      end
22      update  $r.stage2\_sched\_value \leftarrow V_r^{(2)}$ 
23    end
24  end
    // (3) dynamic token limit
25  update  $N_{\max} \leftarrow G_{avail}$  by (27)-(32)
26   $N_{\max} = \max(N_{\max}, \beta_{low} \cdot target\_max)$ 
27   $N_{\max} = \min(N_{\max}, \beta_{high} \cdot target\_max)$ 
    // (4) queue ranking
28  sort(queues) by
     $r.sched\_value + \alpha \cdot (r.waiting\_time)$ 
    // (5) schedule: running  $\Rightarrow$  swapped  $\Rightarrow$ 
    waiting_resume & waiting_new
29   $scheduled \leftarrow \emptyset$  { $scheduled$  is the running batch of
    the current step}
30  foreach  $Q \in queues$  do
31    foreach  $r \in Q$  do
32      if  $scheduled\_tokens < N_{\max}$  then
33         $scheduled \leftarrow scheduled + r$ 
34        update  $r.waiting\_time$ 
35      end
36      else
37        break //  $scheduled$  is full
38      end
39    end
40  end
    // (6) execute one iteration
41  forward( $scheduled$ )
42 end

```

Table 6: Goodput (req/s) comparison of vLLM, InferCept, and *AugServe* under different request rates and arrival burstiness (CV) on Merge and ToolBench datasets with OPT-13B and an H800 GPU.

Datasets	Request rate	CV	vLLM	InferCept	<i>AugServe</i>
Merge	2.0	1	0.22	0.28	0.87
		1.5	0.10	0.13	1.15
		2	0.05	0.08	0.47
	3.0	1	0.15	0.20	1.16
		1.5	0.07	0.11	0.58
		2	0.04	0.06	0.35
ToolBench	3.0	1	2.91	2.80	2.92
		1.5	0.16	0.10	2.04
		2	0.11	0.05	1.39
	4.0	1	2.81	1.06	3.90
		1.5	0.14	0.07	1.65
		2	0.08	0.05	1.51

increases, the attainment of vLLM and InferCept declines sharply. For example, on ToolBench, when the load increases from 4.0 to 5.0 req/s, vLLM’s attainment drops from 98.4% to 22.7%, a nearly fivefold decrease, while InferCept drops from 28.3% to 14.0%. In contrast, *AugServe* still maintains 63.8% under the same condition. This indicates that *AugServe* significantly meets service-level objectives under high load, maintaining service quality far superior to the baselines.

Table 7: SLO attainment (%) comparison of vLLM, InferCept, and *AugServe* under different request rates on Merge and ToolBench datasets with OPT-13B and an H800 GPU.

Datasets	Merge dataset			ToolBench dataset		
Request rate	2.0	3.0	4.0	4.0	5.0	6.0
vLLM	19.5	13.8	9.7	98.4	22.7	17.8
InferCept	28.3	19.1	14.2	28.3	14.0	9.3
<i>AugServe</i>	54.3	51.3	45.8	100.0	63.8	50.1

B.2.2 Workloads with Fixed Time

To more fairly compare the effective throughput performance of *AugServe* with the two baseline systems, we also report the SLO attainment under the same experimental conditions as in §5.2, as well as the goodput at 5× SLOs. All experiments are run for 30 minutes under different load conditions, with the results shown in Figures 11 and 12. It is clear that, under different evaluation metrics, *AugServe* achieves significantly higher SLO attainment and goodput than vLLM and InferCept, demonstrating better effective throughput performance, which is consistent with the results in §5.2.

Summary. Across various metrics, *AugServe* consistently achieves significantly higher SLO attainment and goodput compared to the two baselines.

B.3 Tail Latency Performance

To demonstrate the stability of the system’s latency performance and user experience, we further analyze the P95 TTFT and P95 normalized latency performance of the system under different loads. The experimental setup is consistent with §5.2, and the results are presented in Figures 13 and 14. Specifically, the tail latency of vLLM and InferCept increases gradually as the load increases, indicating that these systems face severe queuing delays and resource contention issues under high load, which leads to performance degradation. In contrast, *AugServe* maintains low tail latency and good stability, providing a better user experience.

Summary. *AugServe* maintains better stability and lower tail latency than vLLM and InferCept under high load, ensuring an enhanced user experience.

B.4 Influence of TPOT

We analyze the time-per-output-token (TPOT) of different systems to compare the computational efficiency across various inference systems under different loads and datasets. The experimental setup is consistent with §5.2. As shown in Figure 15, vLLM uses a single discard-and-recompute policy, which leads to higher memory consumption and computational time, resulting in higher TPOT latency. Meanwhile, InferCept dynamically chooses context handling policies considering the characteristics of augmented LLM request inference, demonstrating superior TPOT latency. *AugServe* goes a step further by employing dynamic scheduling and batch processing strategy, more effectively allocating computational resources and reducing computation latency.

Summary. *AugServe* optimizes TTFT while maintaining excellent TPOT performance, showcasing exceptional computational efficiency.

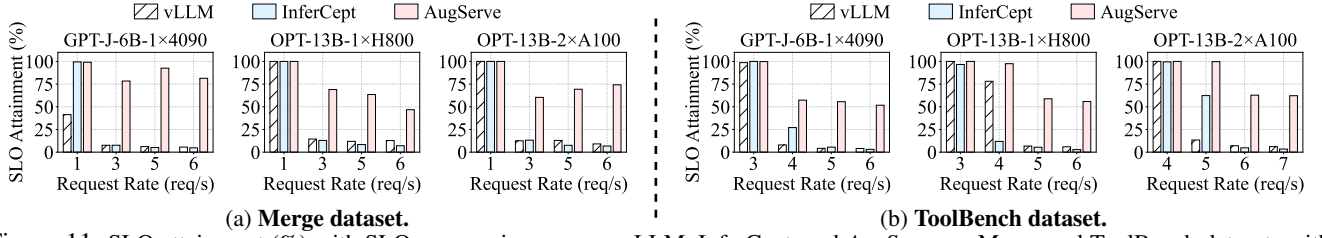


Figure 11: SLO attainment (%) with SLOs comparison among vLLM, InferCept, and *AugServe* on Merge and ToolBench datasets with different models and GPUs. Higher is better.

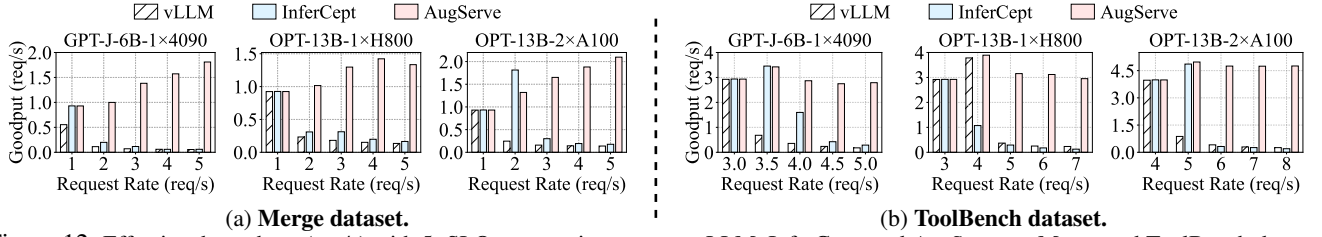


Figure 12: Effective throughput (req/s) with 5xSLOs comparison among vLLM, InferCept, and *AugServe* on Merge and ToolBench datasets with different models and GPUs. Higher is better.

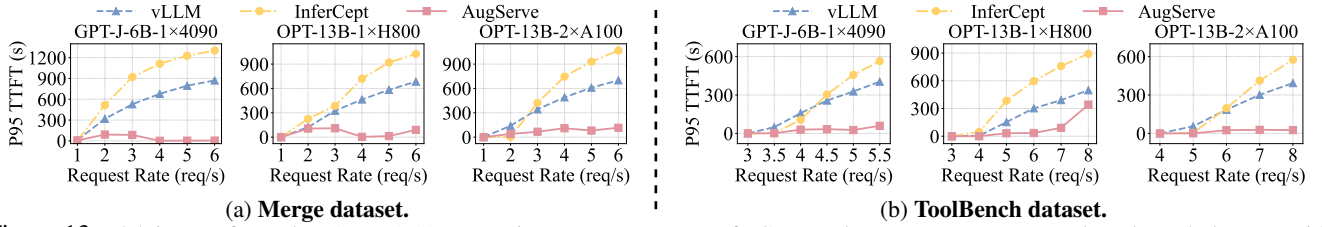


Figure 13: P95 time-to-first-token (TTFT) (s) comparison among vLLM, InferCept, and *AugServe* on Merge and ToolBench datasets with different models and GPUs. Lower right is better, i.e., shorter response time and queueing time.

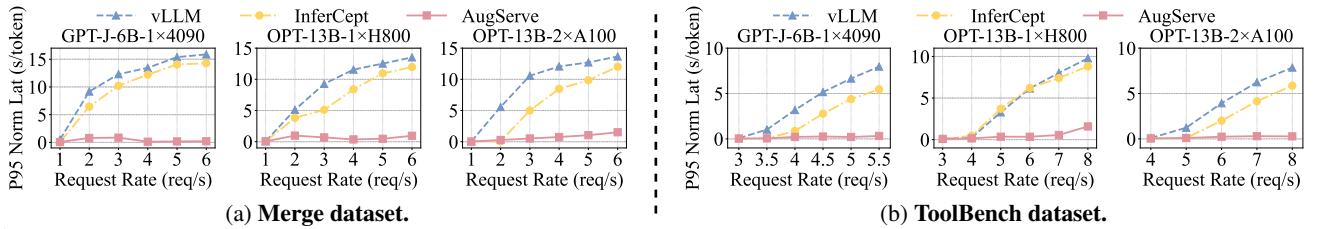


Figure 14: P95 token Latency (s/token) comparison among vLLM, InferCept, and *AugServe* on Merge and ToolBench datasets with different models and GPUs. Lower right is better, i.e., sustains higher serving load.

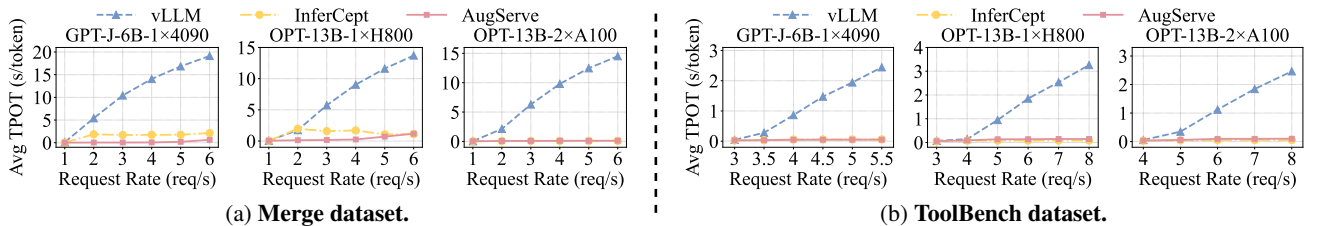


Figure 15: Average time-per-output-token (TPOT) (s/token) comparison among vLLM, InferCept, and *AugServe* on Merge and ToolBench datasets with different models and GPUs. Lower right is better, i.e., sustains higher serving load.